Journal of Physics:
Conference Series

PAPER • **OPEN ACCESS**

Experimental characterization of a variable-pitch Wells turbine

To cite this article: Fabio Licheri *et al* 2024 *J. Phys.: Conf. Ser.* **2893** 012131

Journal of Physics: Conference Series **2893** (2024) 012131 doi:10.1088/1742-6596/2893/1/012131

Experimental characterization of a variable-pitch Wells turbine

Fabio Licheri[1], Tiziano Ghisu[1], Francesco Cambuli[1] and Pierpaolo Puddu[1]

[1]Department of Mechanical, Chemical and Materials Engineering (DIMCM), University of Cagliari, Cagliari, Italy

E-mail: fabio.licheri@unica.it

Abstract. Wells turbines coupled with systems based on the oscillating water column (OWC) principle represent a convenient solution for sea-wave energy conversion. The possibility to operate under the bi-directional airflow that is established within OWC systems is obtained with a symmetrical blade profile staggered at 90 degrees with respect to the turbine's axis of rotation, resulting in a highly reliable machine. On the other hand, the limited operating range represents a relevant drawback which can be overcome introducing a variable-pitch control of the rotating blades. This control solution has been only marginally investigated with experiments, due to the complexity of devising a mechanism capable to change the stagger angle of the rotating blades.

In this work, a Wells turbine prototype with variable-pitch blades has been built and preliminary investigations are presented, with the aim of characterizing its aerodynamic behavior for different blade stagger angles. The performance of the turbine have been evaluated under regular-wave conditions, for different blade-pitch angles, in order to obtain the information required to define the pitch laws for the maximization of rotor performance.

Nomenclature

Acronyms

CFD	computational fluid dynamics
DIMCM	department of Mechanical, Chemical and Materials Engineering
OWC	oscillating water column
PTO	power-take-off

Dimensional properties

α	angle of the absolute flow
β	angle of the relative flow
C	absolute velocity
c	blade chord
D	turbine diameter
f	frequency
γ	blade pitch angle
I	moment of inertia
i	angle of incidence
μ	dynamic viscosity
Ω	angular rotational frequency
p	pressure
Q	volumetric flow rate
r	turbine radius
ρ	air density
s	stall
t	time
$\mathcal{T}$	torque
T_w	piston period
U	peripheral rotor speed
W	relative velocity

Z	piston position
Non-dimensional properties	
η	efficiency
ν	hub-to-tip ratio
p^*	pressure drop coefficient
ϕ	flow coefficient
$\mathcal{T}^*$	torque coefficient
z	number of blades

Subscripts and superscripts	
1	inlet
2	outlet
hub	turbine hub
$meas$	measured
tip	turbine tip
w, f	windage and friction
z	axial direction

1 Introduction

As the demand of renewable energy constantly grows, wave energy becomes even more interesting due to its wide spread availability [1] and predictability. Among the various solutions proposed, systems based on the Oscillating Water Column (OWC) principle are the most promising [2] due to their simplicity and reliability. OWC devices are made of two main parts: an air chamber where the wave motion is converted into the pneumatic energy of a bi-directional air flow through a duct connected to the atmosphere, and a power-take-off (PTO) that converts this pneumatic energy into mechanical energy on its shaft. Finally, an electric generator converts the mechanical energy into electricity.

Air turbines have typically been used as PTOs, although the bi-directional nature of the airflow requires a rectifying system to feed conventional rotors. The Wells turbine [3] configuration overcomes this limitation thanks to the symmetrical blade profile, staggered at 90 degrees with respect to the axis of rotation, which results in a constant direction of the output torque regardless of the flow direction. The self-rectifying behavior, obtained with a relatively simple construction, is certainly the most interesting feature of this turbine. On the contrary, a number of drawbacks exist, in particular a limited operating range due to stall.

Different solutions have been proposed to delay the occurrence of stall: a row of guide vanes on both sides of the rotor can be used to adjust the incidence angle of the flow, not only to increase the operating range, but also to improve rotor performance [4, 5, 6]; speed-controlled Wells turbines have been studied [7, 8] and tested [9, 10] showing the effectiveness of this action in delaying stall while maximizing rotor performance. Rotors with variable-pitch blades represent an ambitious solution for controlling the incidence angle, through the modification of the blades' stagger angle during turbine operation. Numerical studies have shown the capability of pitch-controlled Wells turbines to operate in the absence of stall while maximizing performance under irregular wave motion [11], both considering passive and active control strategies [12]. Information on Wells turbine performance at various pitch angles have been obtained both numerically [12, 13] and experimentally [13, 14], mainly under stationary flow conditions.

This paper introduces a Wells turbine prototype with variable-pitch blades built in the Department of Mechanical, Chemical and Materials Engineering (DIMCM) at the University of Cagliari. The blades of the rotor can be oriented by an external stepper motor to simultaneously modify their stagger angle. Preliminary experimental investigations are presented in this work, with the aim of characterizing the Wells turbine aerodynamic behavior for different blade stagger angles. These performance measurements have been conducted under regular wave conditions, providing a complete description of the rotor aerodynamic behavior even beyond the stall point.

2 Turbine performance definition

Wells turbine performance is typically evaluated [15] in non-dimensional form, defining the flow coefficient ϕ, the torque coefficient T^*, the wall pressure coefficient p^* and the efficiency η as follows:

$$\phi = \frac{C_z}{\Omega r_{tip}} \qquad \mathcal{T}^* = \frac{\mathcal{T}}{\rho \Omega^2 r_{tip}^5} \qquad p^* = \frac{\Delta p}{\rho \Omega^2 r_{tip}^2} \qquad \eta = \frac{\mathcal{T}\Omega}{\Delta p Q} \tag{1}$$

where C_z is the axial flow velocity at the turbine inlet responsible for the flow rate, Q, and Δp is the static pressure drop across the turbine.

All the non-dimensional parameters above can be evaluated by means of global measurements only, i.e. the turbine rotational speed and its output torque, the wall static pressures at both sides of the turbine and the flow rate, based on which the flow speed is evaluated. In the present work, the measured torque $\mathcal{T}_{meas}$ has been cleared from windage and friction losses and from rotor inertial torque, based on the following balance of moments applied at the rotor shaft:

$$\mathcal{T}_{meas} = \mathcal{T} + \mathcal{T}_{w,f} + I\frac{\mathrm{d}\Omega}{\mathrm{d}t} \tag{2}$$

where $\mathcal{T}_{w,f}$ is the windage and friction torque contribution and I is the moment of inertia of the rotor, as described in Sec. 3. Thus, the non-dimensional torque coefficient is calculated using the aerodynamic torque $\mathcal{T}$ and the efficiency of the turbine corresponds to its aerodynamic one [16].
Figure 1 shows the velocity triangles at inlet and outlet of a Wells turbine blade in the presence of a positive pitch angle, γ.

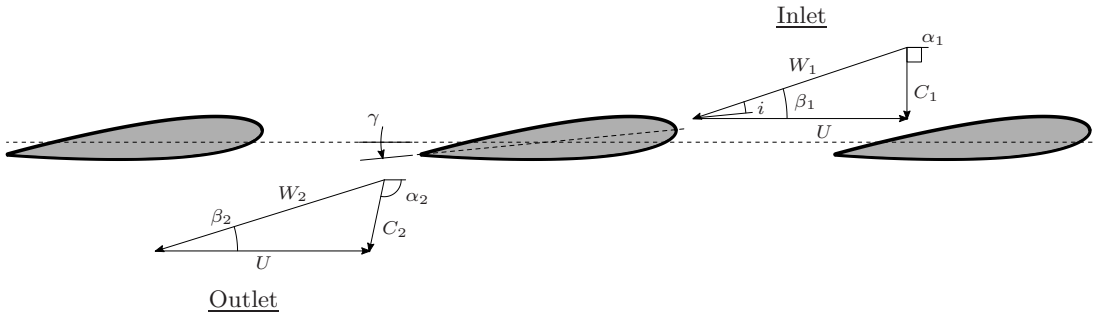

Figure 1: Velocity triangles for a variable pitch Wells blade.

In this representation, positive values of γ result in a lower incidence angle on the blade profile, hence the stall onset is expected to occur for larger values of the flow coefficient $\phi = \arctan(\beta_1)$. It is worth to note that when the blade profiles rotate with respect to the incoming flow, a physical blade passage is created between two adjacent blades, which can not be identified when the blade is staggered orthogonally to the axis of rotation. This may further delay stall to higher values of the flow coefficient.

3 Experimental apparatus and methodology

The OWC simulator housed at the DIMCM is schematically reproduced in Fig. 2, together with a close-up view of the measuring section where the turbine is installed.
The experimental apparatus is composed of a cylindrical steel chamber where a piston, driven by a hydraulic unit, reproduces the periodic motion of a water column inside an OWC. Different wave states can be reproduced with this experimental setup by changing the amplitude and frequency of the periodic motion of the piston, limited to a maximum flow speed ≈ 20 m/s at the inlet of the rotor.
A linear wire potentiometer is employed to measure the piston displacement and for feedback control of the hydraulic unit. Above the chamber, a Wells turbine, which drives an electric generator controlled by an inverter with encoder feedback, is installed. The Wells turbine used for these experiments is equipped with a mechanism that modifies the blade stagger angle by rotating simultaneously the 14 blades of the rotor around an axis. The blades have been made of a 3D printed resin and have been assembled to the rotor with rod connections. A shaft-to-shaft torque sensor is placed between the turbine and the electric machine, and it also allows to measure the turbine rotational speed with a built-in optical encoder. The measuring section is provided with wall pressure taps placed on both rotor sides at a distance of ± 7.5 mm from the blade chord. The volumetric flow rate is calculated based on the piston motion (recorded with the linear potentiometer), taking into account the area ratio between OWC chamber and turbine duct, and the time delay between piston speed and corresponding flow speed at the rotor inlet, due to the presence of the chamber volume [17]. Based on this calculation, the inlet flow velocity C_z used in Eqns. (1) is calculated assuming a uniform distribution along the blade radius.
The variable-pitch rotor, whose main geometric characteristics are listed in Tab. 1, has been characterized in terms of its global performance, as introduced in Sec. 2 and under regular wave conditions.
With the aim of defining the performance of the Wells turbine for different values of the blade stagger angle, a sinusoidal piston displacement has been reproduced with the OWC simulator. The acquisition time for each test has been set to record signals for at least 20 piston periods with a sampling rate of 250 Hz. A zero crossing method has been applied to the piston position signal, in order to identify the piston periods. The acquired signals have then been averaged with a phase locked process. Finally, the obtained signals have been re-sampled, equally spacing 250 points with linear interpolation. This

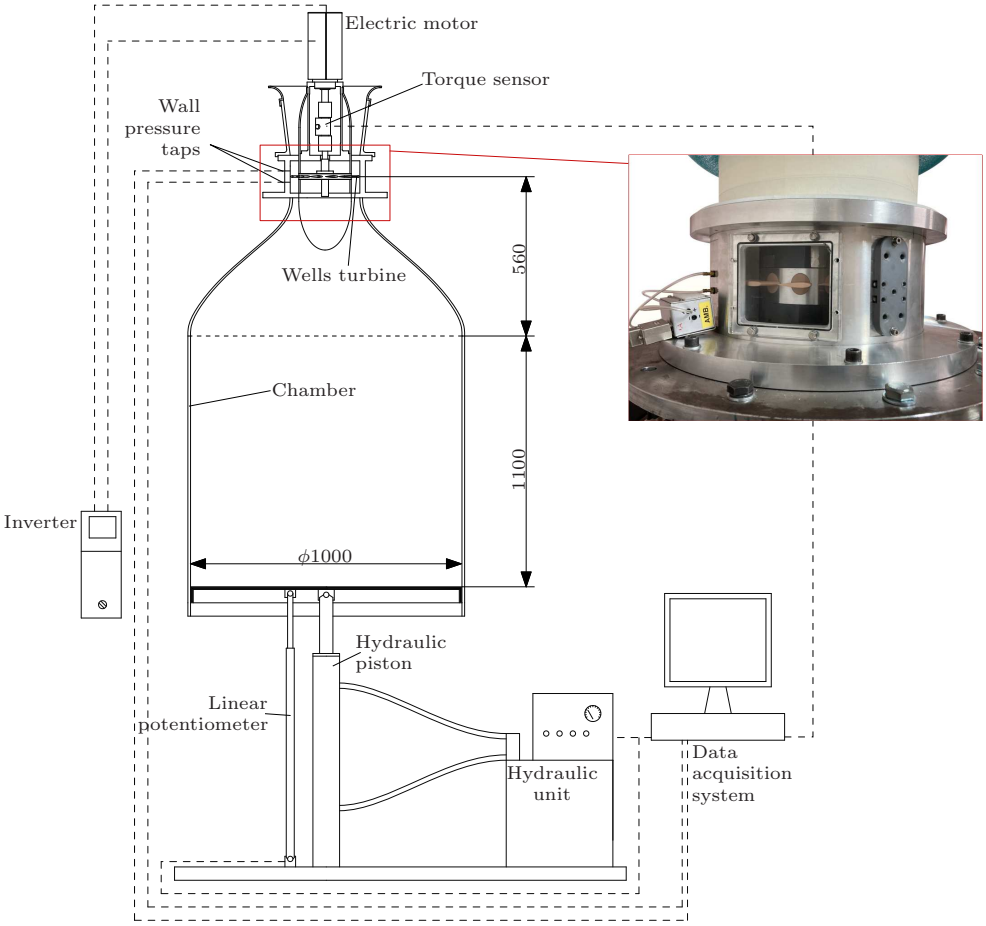

Figure 2: Experimental setup scheme and measuring section.

Table 1: Geometric parameters of the variable-pitch Wells turbine.

rotor tip diameter, D_{tip}	249.4 mm	airfoil profile	NACA 0015
rotor hub diameter, D_{hub}	190 mm	solidity	0.729
tip clearance	1.3 mm	sweep ratio	15/36
chord length, c	36 mm	hub-to-tip ratio, ν	0.76
number of blades, z	14	blade stagger angle, γ	$\pm$7 deg

procedure has been shown to be sufficient to correctly describe the measurements' histories over a period, as shown in Fig. 3.
Maximum relative uncertainties for the global measurements are the following:

- $\pm$1.0 % for the wall static pressure drop,
- $\pm$7.9 % for the output torque,
- $\pm$0.1 % for the piston position,
- $\pm$0.15 % for the rotational freqeuency.

Due to the presence of a swirl flow at the rotor inlet during the outflow phase, only the inflow phase has been considered to determine the rotor performance, as during this phase the inlet flow has been proved to be fully axial [18, 19]. Several positive blade setting angles have been tested. The wave period and

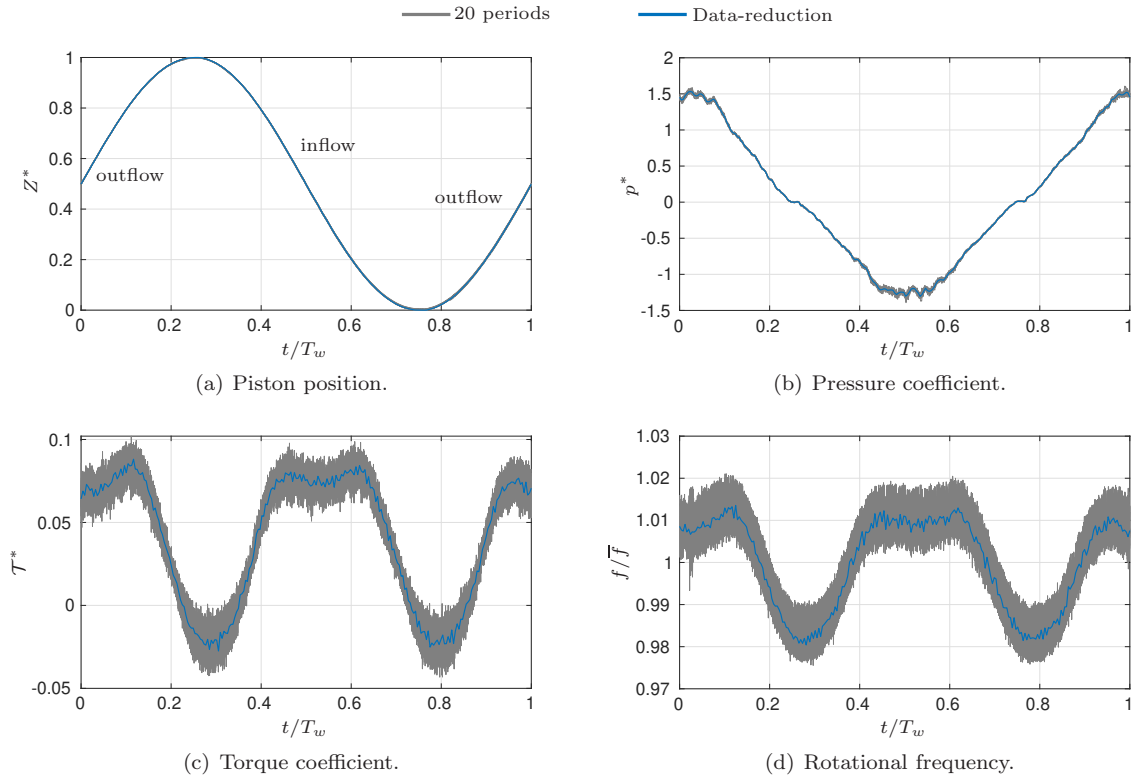

(a) Piston position.

(b) Pressure coefficient.

(c) Torque coefficient.

(d) Rotational frequency.

Figure 3: Measured quantities in one piston period and phase-averaged result.

the turbine's rotational speed have been adjusted in order to extend the flow coefficient range beyond the stall conditions. A maximum value of the Reynolds' number based on the blade chord, i.e. $Re_c = (\rho\, c\, W_1)/\mu$, of about 7.5×10^4 has been reproduced for all the tests, with a maximum variation of ± 2 % among all tests.
Preliminary measurements of windage and friction losses and inertial torque have been performed in the selected range of variation for the blade stagger angle (see Tab. 1). Windage and friction losses, measured under no-load conditions for several fixed values of the rotational speed, have shown no significant differences with γ, hence an averaged correlation between the rotational speed and the losses has been established and used. Analogously, the inertial moment of the rotating parts, evaluated under no-load conditions by setting ramps for the rotational speed, does not vary with γ and a single value of $I = 1.05 \times 10^{-2}$ [kg·m^2] has been assumed for all values of the stagger angle.

4 Results

Global performance for different values of the pitch angle is shown in Fig. 4, in the form of pressure and torque coefficients as a function of the flow coefficient.
As expected, the variation of the blade stagger angle results in a reduced pressure drop across the rotor for the same flow coefficient, as evident in Fig. 4 (a). These different characteristic curves result from different rotor cascades obtained by varying the blade stagger angle. Similarly, torque coefficient trends show lower values of the aerodynamic torque as γ becomes larger, for the same operating condition, although these differences are less significant than the previous ones. On the other hand, the extension of the stable operating range, in the absence of stall, is evident by observing Fig. 4 (b). A relatively small variation of γ from 0 to 7 degrees doubles the flow coefficient at stall, from $\phi_s = 0.31$ to 0.63. This evidence can be also observed if the value of the flow coefficient at stall ϕ_s is reported as a function of the blade stagger γ, as done in Fig. 5 (a).
In the same figure, a theoretical flow coefficient at stall, calculated as $\arctan\left((\beta_{1,s})_{\gamma=0} + \gamma\right)$, is also reported (dashed red line), highlighting the non-linear contribution provided by the blade cascade effect. In Fig. 5 (b), the same information is provided in terms of the mean incidence angle $\overline{i}$. It should be stressed that this does not represent the actual local flow incidence, given flow non-uniformities

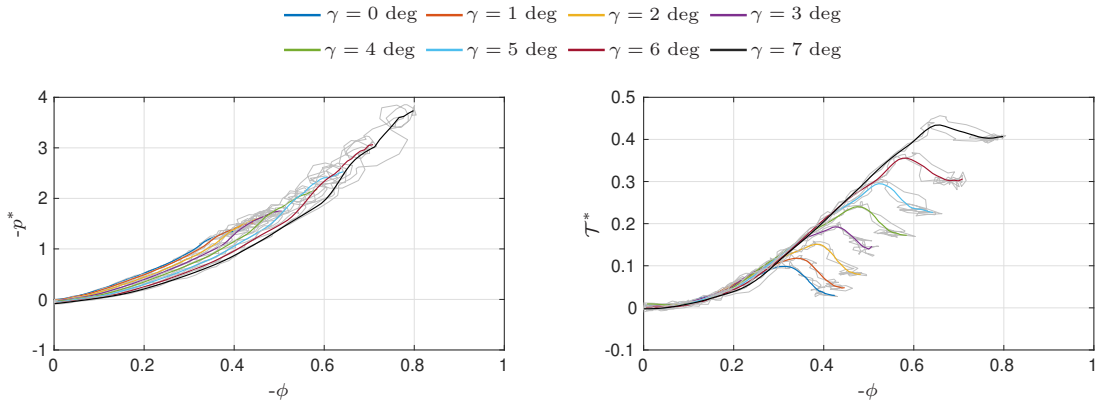

(a) Pressure coefficient. (b) Torque coefficient.

Figure 4: Performance coefficients for different blade stagger angles as a function of the flow coefficient.

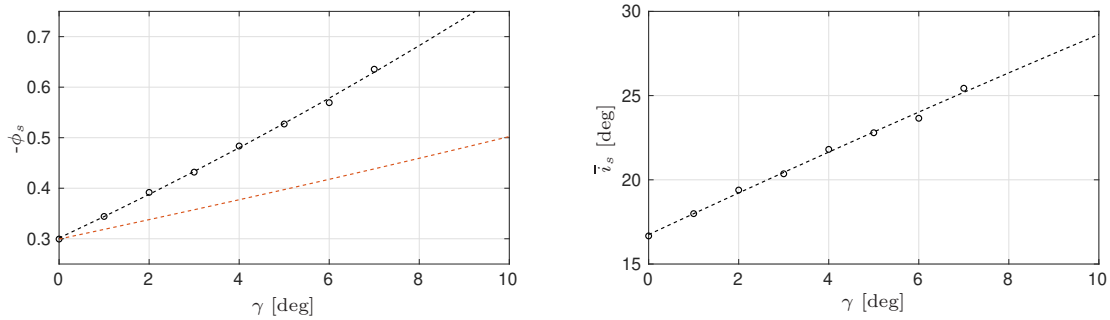

(a) Flow coefficient at stall. (b) Mean incidence angle at stall.

Figure 5: Stall limit correlations.

associated to the the leakage flow and to the variable solidity along the blade radius.
The same guidance effect has been observed in previous 2D computational fluid dynamics (CFD) simulations conducted on the same rotor geometry [12]. Although 2D CFD in [12] predicts the stall occurrence for sensibly lower values of the flow coefficient (due to the absence of the tip leakage flow in 2D simulations), it is interesting to compare the trend of the flow coefficient at stall, generalized with respect to its value for the conventional Wells rotor, with the blade pitch-angle, as done in Fig. 6.

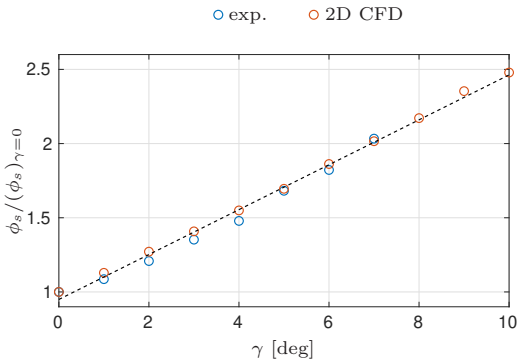

Figure 6: Stall point comparison between experiments and 2D CFD in [12].

Correlations of Fig. 6 show that the rate of variation of the flow coefficient at stall is well predicted

using simple 2D CFD simulations, with maximum differences with respect to experiments lower than 5% (in the investigated range of γ). This result also suggests that the guidance effect is well predicted with 2D simulations and is responsible of the progressive delay of stall with γ. Moreover, the good agreement between experiments and numerical simulations, shown in Fig. 6, allows to define a variable-pitch law for maximizing the energy production, as proposed in [12], using only numerical results, taking into account a correction for the stall angle of the zero-pitched Wells rotor, $\phi_{s,0}$.
Finally, it is interesting to evaluate the efficiency of the tested rotor with different blade stagger angles, as defined in Eqn. (1). Figures 7 (a) and (b) show the aerodynamic efficiency as a function of the flow coefficient and the pressure coefficient, respectively.

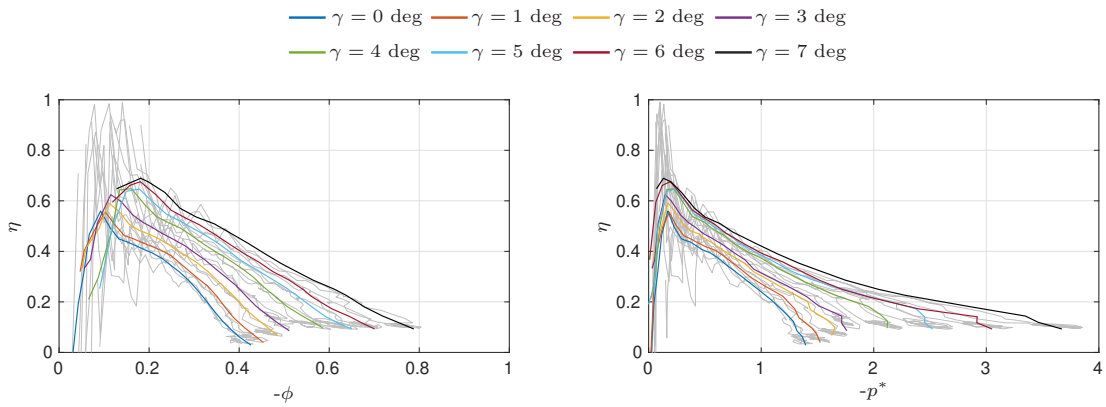

(a) Efficiency vs flow coefficient.

(b) Efficiency vs pressure coefficient.

Figure 7: Instantaneous efficiency of the turbine for different blade stagger angles.

The maximum rotor aerodynamic efficiency grows with the pitch angle γ and it occurs for larger values of the flow coefficient, as already observed for the maximum torque coefficient. Nevertheless, the maximum efficiency does not occur just before the stall point (as for the maximum value of $\mathcal{T}^*$), but it is obtained for sensibly lower values of the flow coefficient. This result, already observed for fixed geometry Wells turbines [10], is caused by the rapid increase in p^* and by the simultaneous reduction in the slope of the $\mathcal{T}^*$ curve, at large values of the flow coefficient, even before the maximum value of $\mathcal{T}^*$ is reached. The maximum value of the torque coefficient (just before stall) occurs at larger values of flow coefficient than the maximum efficiency value, as common in aerodynamic profiles [20] and turbomachinery [21].
This trend of the aerodynamic efficiency suggests a different pitch control-law for maximizing the turbine efficiency instead of the output torque. A control law performed to maximize the output torque, hence the energy produced by the turbine, allows to extend the operating range with a lower variation of the blade pitch angle with respect to the control law based on efficiency maximization. Another interesting result, is shown in Fig. 7 (b), where the maximum efficiency for different values of γ is obtained for an almost constant value of the pressure coefficient p^*. Given that the pressure drop drives directly the flow through the turbine in an OWC, it can be deduced that a variable pitch Wells turbine has the potential to provide significantly larger efficiencies, in combination with larger operating ranges.

5 Conclusions

This paper presents preliminary experimental results on a variable-pitch Wells turbine prototype coupled with a OWC simulator housed at the DIMCM of the University of Cagliari. The turbine prototype is equipped with a mechanism capable to vary the blade pitch-angle of the rotor-blades during its operation, with the aim to avoid stall inception and increase the stable operating range of the Wells rotor. The Wells turbine has been characterized by evaluating its global performance under regular-wave conditions while fixing a blade-pitch angle between 0 and 7 degrees.
Based on the results presented in this work, the following considerations can be drawn:

- The effectiveness of a variable-pitch control strategy to extend the stable operating range of a conventional Wells rotor delaying stall occurrence has been demonstrated based on experimental results. It has been observed how a relatively small variation of the pitch angle almost doubles the flow coefficient at stall, resulting in a wider stable operating range.

- The mean incidence angle at stall, that does not represent the local flow incidence on the blade profile, has been observed to progressively grow due to the presence of the guidance effect, which becomes even more relevant as the pitch angle increases.
- The comparison between the experimental results and the numerical ones obtained for a rotor with the same solidity using 2D CFD [12], has shown good agreement in predicting stall trends for different pitch angles. This suggests that variable pitch control laws can be established using less expensive CFD simulations, only taking into account a correction for the stall point of the reference (non-staggered) Wells turbine, due to the difficulty of predicting the stall occurrence using (not only) 2D numerical schemes.

Local investigations, based on experimental or numerical methods, will give more information on the flow at stall occurrence for different pitch angles, quantifying the guidance effect and its variation with the blade stagger angle.

Funding
This study was carried out by Fabio Licheri within the "e.INS - Ecosystem of Innovation for Next Generation Sardinia" funded by the Italian Ministry of University and Research under the Next-Generation EU Programme (National Recovery and Resilience Plan - PNRR, M4C2, INVESTMENT 1.5 - DD 1056 of 23/06/2022, ECS00000038). This manuscript reflects only the authors' views and opinions, neither the European Union nor the European Commission can be considered responsible for them.
Francesco Cambuli and Tiziano Ghisu acknowledge financial support under the National Recovery and Resilience Plan (NRRP), Mission 4, Component 2, Investment 1.1, Call for tender No. 1409 published on 14.9.2022 by the Italian Ministry of University and Research (MUR), funded by the European Union - NextGenerationEU - Project Title APEIRON - CUP F53D23009560001 - Grant Assignment Decree No.0001385 adopted on 01-09-2023 by the Italian Ministry of Ministry of University and Research (MUR).

References

[1] Gunn K, Stock-Williams C. Quantifying the global wave power resource. Renewable Energy. 2012;44:296-304.

[2] Curto D, Franzitta V, Guercio A. Sea wave energy. A review of the current technologies and perspectives. Energies. 2021;14(20).

[3] Wells A. Fluid Driven Rotary Transducer - BR. Pat. 1595700 [Patent]; 1976.

[4] Gato LMC, de O Falcão AF. Performance of the Wells turbine with a double row of guide vanes. JSME international journal Ser 2, Fluids engineering, heat transfer, power, combustion, thermophysical properties. 1990;33(2):265-71.

[5] Takao M, Setoguchi T, Kim TH, Kaneko K, Inoue M. The performance of Wells turbine with 3D guide vanes. International Ocean and Polar Engineering Conference; 2000. p. ISOPE-I00055.

[6] Govardhan M, Dhanasekaran TS. Effect of guide vanes on the performance of a self-rectifying air turbine with constant and variable chord rotors. Renewable Energy. 2002;26(2):201-19.

[7] Amundarain M, Alberdi M, Garrido AJ, Garrido I, Maseda J. Wave energy plants: Control strategies for avoiding the stalling behaviour in the Wells turbine. Renewable Energy. 2010;35(12):2639-48.

[8] Lekube J, Garrido AJ, Garrido I. Variable speed control in Wells turbine-based oscillating water column devices: optimum rotational speed. IOP Conference Series: Earth and Environmental Science. 2018 mar;136(1):012017.

[9] Licheri F, Ghisu T, Cambuli F, Puddu P. Wells turbine efficiency improvements: Experimental application of a speed control strategy. Journal of Physics: Conference Series. 2022;2385(1).

[10] Licheri F, Puddu P, Cambuli F, Ghisu T. Experimental investigation on a speed controlled Wells turbine for wave energy conversion. International Conference on Offshore Mechanics and Arctic Engineering. 2022 06;Volume 8: Ocean Renewable Energy:V008T09A077.

[11] Sarmento AJNA, Gato LMC, de O Falcão AF. Turbine-controlled wave energy absorption by oscillating water column devices. Ocean Engineering. 1990;17(5):481-97.

[12] Licheri F, Climan A, Puddu P, Cambuli F, Ghisu T. Numerical study of a Wells turbine with variable pitch rotor blades. Energy Procedia. 2018;148:511-8.

[13] Gato LMC, de O Falcão AF. Aerodynamics of the Wells turbine: Control by swinging rotor-blades. International Journal of Mechanical Sciences. 1989;31(6):425-34.

[14] Kim TH, Setoguchi T, Takao M, Kaneko K, Santhakumar S. Study of turbine with self-pitch-controlled blades for wave energy conversion. International Journal of Thermal Sciences. 2002;41(1):101-7.

[15] Gato LMC, de O Falcão AF. Aerodynamics of the Wells turbine. International Journal of Mechanical Sciences. 1988;30(6):383-95.

[16] Licheri F, Cambuli F, Puddu P, Ghisu T. A comparison of different approaches to estimate the efficiency of Wells turbines. Journal of Fluids Engineering. 2021 02;143(5).

[17] Paderi M, Puddu P. Experimental investigation in a Wells turbine under bi-directional flow. Renewable Energy. 2013;57:570-6.

[18] Licheri F, Ghisu T, Cambuli F, Puddu P. Detailed investigation of the local flow-field in a Wells turbine coupled to an OWC simulator. Renewable Energy. 2022;197:583-93.

[19] Licheri F, Ghisu T, Cambuli F, Puddu P. Experimental reconstruction of the local flow field in a Wells turbine using a three-dimensional pressure probe. Energy. 2024;296:131062.

[20] Abbott IH, von Doenhoff AE. Theory of Wing Sections. New York: Dover; 1959.

[21] Lopez DI, Ghisu T, Shahpar S. Global Optimization of a Transonic Fan Blade Through AI-Enabled Active Subspaces. Journal of Turbomachinery. 2021 09;144(1):011013.